Bulgarian Chemical Communications, Volume 58, Issue 4 (pp. 436-441) 2026 *DOI: 10.34049/bcc.58.4.5739*

Design and biological evolution of La_2O_3-ZnO mixed metal oxide nanomaterials for anticancer activity against MCF-7 cell lines

A. R. Padol[1], M. E. Navgire[2], M. A. Raut[3]*

[1]*Dr. Rafiq Zakaria College for Women, Chh. Sambhajinagar, 431003 India*
[2]*Jijamata College of Science and Arts, Bhende Bk. Ahilyanagar, India*
[3]*Pratisthan Mahavidyalaya, Paithan, Chh. Sambhajinagar, India*

Received: December 14, 2025; Revised: May 25, 2026

Nanotechnology-based mixed metal oxide nanocomposites have gained significant attention in biomedical applications owing to their enhanced physicochemical and therapeutic properties. In the present study, La_2O_3–ZnO mixed oxide nanoparticles were synthesized by a co-precipitation method and evaluated for their *in-vitro* anticancer activity against MCF-7 human breast cancer cells. Structural and morphological characterization was carried out using XRD, UV-DRS, FTIR and SEM techniques. The XRD analysis confirmed the crystalline nature of the synthesized nanocomposite with an average crystallite size of 30.79 nm. The UV-DRS analysis revealed optical band gap energy of 3.21 eV for the La_2O_3-ZnO nanocomposite. FTIR spectra confirmed the formation of La–O and Zn–O bonds while SEM images demonstrated a porous nanocrystalline morphology. Cytotoxicity study using the MTT assay showed a dose-dependent reduction in MCF-7 cell viability which decreased from 97.11 ± 6.54% to 17.04 ± 1.22% with increasing nanoparticle concentration (1–50 µg/mL). Morphological studies further confirmed cellular deformation and apoptotic changes after nanoparticle treatment. The obtained results indicate that La_2O_3–ZnO mixed oxide nanoparticles exhibit promising anticancer potential and may serve as effective alternative nanotherapeutic agents for breast cancer treatment.

Keywords:-La_2O_3–ZnO nanocomposite; anticancer activity; MCF-7 cells; mixed metal oxide; nanotechnology

INTRODUCTION

In the recent years considerable attention is paid to the field of nanoscience and nanotechnology. A variety of applications in the field of material sciences, medicine, computer sciences and environmental studies such as pollution was studied. The synthesis of nanomaterial-based anticancer and antimicrobial agents has gained considerable attention owing to their fundamental, distinctive physico-chemical and biological properties resulting from the small size and large surface area. Anticancer agents synthesized from nanomaterials and nanocomposites have shown much better stability under different physical conditions such as temperature, pressure and mass-to-volume ratio compared to organic-based anticancer agents [1-5]. In the past few years a variety of studies has been performed to investigate the anticancer activity of metal oxides, mixed metal oxides and their composites [6-13].

A number of research papers on cytotoxic (anticancer) activity is focused on mixed metal oxides [14-17]. Mixed nanocomposite materials, along with surface-active agents such as cetyltrimethyl ammonium bromide (CTAB), PEG and others, are investigated for their cytotoxic effect and anticancer activities, giving a considerable contribution to the development of alternate anticancer agents for the control of cancerous cells. Transition metals, with their important properties such as high melting point, high mass-to-volume ratio, high thermal conductivity and good physico-chemical properties due to their 4f orbital electrons, have been applied in electronic, medicinal, and agricultural studies [18, 19].

Nanotechnology is an emerging research field with agro-industrial, pharmaceutical and medicinal applications [20]. Nanomaterials can disrupt the generation of free radicals through different mechanisms due to their capacity to mimic the activity of enzymes or to donate electrons [21].

Rare earth nanoparticles are used in human healthcare for drug delivery in tumor therapy, bio imaging and diagnosis [22]. The development of this type of nanomaterials can include the use of essential trace elements such as Zn^{2+} which is a safe material exploited for nano biotechnologies due to its optical, biological, mechanical, catalytic and intrinsic therapeutic properties and its easy manipulation in the synthesis of doped nanostructures, e.g. lanthanum doped with zinc [23-29].

In therapeutic applications, zinc-doped nano-particles have been reported to target neurological diseases and to possess biocompatibility with treatment regimens such as chemotherapy and radiotherapy [30, 31]. As compared to other

* To whom all correspondence should be sent:
E-mail: *mahanandaraut@yahoo.in*

© 2026 Bulgarian Academy of Sciences, Union of Chemists in Bulgaria

lanthanide series elements, lanthanum oxide (La_2O_3) is applied to fabricate nanostructures through different physical and chemical methods. Lanthanum is recognized for its important biomedical uses due to its genotoxicity, presence of 4f shielded electrons, biocompatibility, magnetic features and redox switching capacity [32].

This study aims to synthesize and characterize lanthanum-zinc mixed oxide nanoparticles and evaluate their anticancer potential against the MCF-7 breast cancer cell line. The nanoparticles were synthesized by a co-precipitation method, and their cytotoxicity was evaluated using MTT assay, with DOXO serving as the standard reference drug.

MATERIALS AND METHODS

Chemicals and materials

Zinc nitrate, lanthanum nitrate, and ammonia were purchased from Sigma Aldrich. All chemicals were of analytical grade and were used as received.

Synthesis of lanthanum-zinc mixed oxide materials

The synthesis was made using deionized water and 500 ml of precursor salt solution prepared by mixing individual solutions of the two salts such as to contain an overall metal concentration of 0.5 mole l^{-1} and lanthanum-to-zinc molar ratio of 1:4. This solution mixture was slowly added in a beaker under continuous magnetic stirring. At a flow rate of 9 ml min^{-1} ammonia (1:1) was added to keep the pH value of the medium at 10±0.2. An initial volume of 25 ml of water was placed in the beaker before dropping of metallic salts mixture and ammonia solution. After addition of reactants, the solution mixture was aged at ambient temperature for 40 min under continuous stirring. Subsequently, the mixture was ultrasonicated at 40 °C for 30 min. After cooling, the product was centrifuged (10 min at 4000 rpm). Then the product was washed three times with distilled water and dried at 80 °C for 24 h. Synthesized sample was calcined at 650 °C for about 3 h.

Characterizations

- *X-ray diffraction (XRD) analysis.* XRD analysis confirmed that the synthesized La_2O_3-doped ZnO nanocomposite material was crystalline in nature (see Fig. 1). The diffraction of peaks of pure ZnO, shown in Fig. 1(a) with 2θ (°) values of 32.135, 35.083, 37.095, 47.734, 56.75, 63.07 and 70.187 corresponds to (100), (002), (101), (102), (110), (103), and (201) planes, and perfectly match JCPDS card no. 79-0205 with hexagonal phase [33]. Similarly, Fig. 1(b) shows the diffraction peaks of pure La_2O_3 with 2θ (°) values of 22.861, 29.614, 30.960, 44.547 and 54.549, corresponding to (221), (321), (400), (440) and (631) planes, respectively, and perfectly matching JCPDS card no. 04-0856 with cubic phase [34].

Figure 1(c) illustrates the formation of the mixed phase of the La_2O_3-ZnO nanocomposite material. The planes that have (hkl) values of (221), (321), and (440) correspond to La_2O_3 while remaining planes, which have (hkl) values of (100), (002), (101), (102), (110), (103) and (201) correspond to ZnO material. By using Debye-Scherrer equation, the crystallite size of the synthesized nanocomposite material was calculated (Table 1).

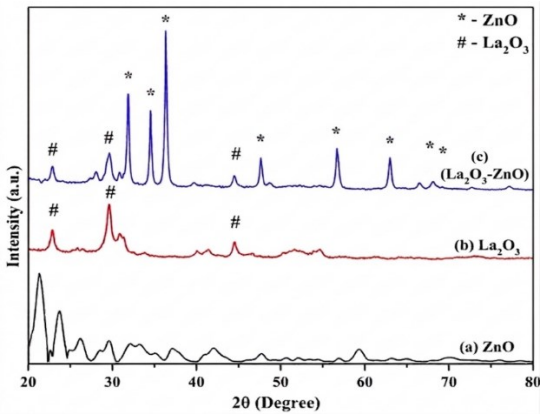


Figure 1. XRD analysis of (a) ZnO, (b) La_2O_3 and (c) La_2O_3-ZnO nanocomposite

Table 1. Crystallite size of synthesized nanocomposite materials.

S. No.	Material	2θ (°)	FWHM (°)	Crystallite size (nm)
1	La_2O_3	29.614	0.8399	10.23
2	ZnO	21.401	0.9741	8.67
3	La_2O_3 -ZnO	36.365	0.2838	30.79

- *Ultraviolet diffuse reflectance spectroscopy (UV-DRS) analysis.* The optical study of the synthesized material was done by UV-DRS analysis, as shown in Fig. 2. The band gap energy was calculated using Kubelka-Munk function [35] with $(F(R)h\vartheta)^2$ $(eV(cm^{-1}))^2$ *versus* energy ($h\vartheta$) shown in Fig. 2. The material shows band gap energy of 3.21 eV for mixed La_2O_3-ZnO nanocomposite material [36].

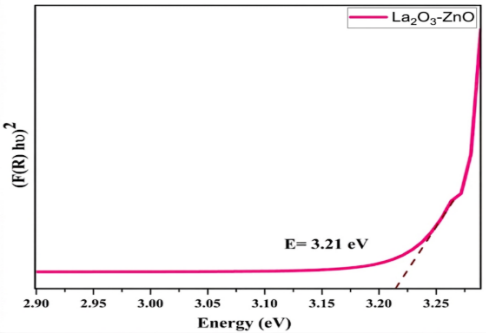


Figure 2. UV-DRS spectrum of La_2O_3-ZnO nanocomposite

- *Fourier transform infrared spectroscopy (FTIR) analysis.* The FTIR spectra of ZnO, La_2O_3 and La_2O_3-ZnO nanocomposite were recorded in the range of 4000–450 cm^{-1} (see Figure 3(a-c)). The sharp peak at 612 cm^{-1} is characteristic of the presence of Zn–O stretching vibrations. The peaks at 1070 and 1429 cm^{-1} are due to C-O stretching vibration and adsorbed carbonate groups, respectively, as shown in Fig. 3(a) [37-40]. The stretching frequencies at 854 and 645 cm^{-1} are primarily due to La-O stretching and bending vibrations, respectively, as shown in Fig. 3(b) [41].

Figure 3(c) shows the FTIR spectrum of La_2O_3-ZnO with characteristic Zn-O stretching vibrations at 499 cm^{-1} and La-O stretching and bending vibrations at 672 and 851 cm^{-1}, which confirms the formation of nanocomposite material [42].

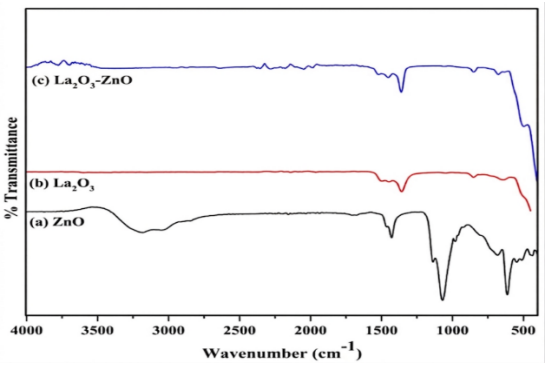


Figure 3. FTIR spectra of (a) ZnO, (b) La_2O_3 and (c) La_2O_3-ZnO nanocomposite

- *Scanning electron microscopy (SEM) analysis.* The surface morphology of La_2O_3-ZnO nanocomposite was tested by SEM analysis to find out the dispersion of the active species on the support. Figure 4 shows SEM images with different resolution, which demonstrate the nanocrystalline structure of the composite material. The increasing porosity and improved morphology of the material is clearly seen.

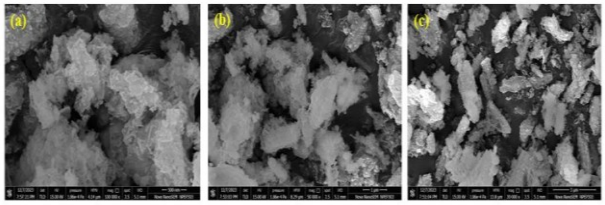


Figure 4. SEM micrographs of (a) ZnO, (b) La_2O_3, and (c) La_2O_3-ZnO nanocomposite

Application for anticancer activity

- *Cytotoxicity against MCF-7 cells using MTT assay.* The MTT cell viability test is a simple, sensitive, quantitative and efficient procedure for counting the number of viable cells in a given culture. This homogeneous colorimetric evaluation works by converting MTT, a pale-yellow substrate, to formazan, a purple dye. This cellular reduction requires the pyridine nucleotide cofactors NADH/NADPH and is only catalyzed by live cells. The formazan product has limited water solubility and appears as purple crystals. Dissolving the resultant formazan in a solubilization buffer allows for easy measurement of its production. The intensity of the product color, measured between 550 and 620 nm, is associated with the number of living cells in the culture. The test kit's reagents were carefully developed and adjusted for sensitivity, assay robustness and automation.
- *Morphological studies.* MCF-7 human breast cancer cell lines were cultured in 25 cm^2-Corning canted neck flasks using DMEM-F12 medium enriched with 20% FBS and 3 mM L-glutamine. This was further supplemented with an antibiotic mixture containing 500 µg/mL of penicillin, 500 µg/mL of streptomycin and 1.25 µg/mL of amphotericin-B to prevent bacterial infections. The cultures were kept in 5% CO_2 humidified atmosphere at 37 °C. For passaging, cells were detached using 0.25% trypsin-1mM EDTA and reseeded in 75 cm^2-flasks at 2.3×10^4 cells/cm^2, with the medium refreshed every two days. Cell confluence of 80% was microscopically verified before conducting experiments 24 h after seeding to avoid cell differentiation. Et-16 and Et-20 refer to synthetic anti-neoplastic ether lipids (specifically, alkyl-lysophospholipid analogues) treatments were applied at their IC_{50} concentrations 24 h post-seeding, with observations and imaging done 24 h post-treatment using an Axiovert 200M phase contrast microscope at 10× magnification utilizing Axiovision Rel.4.2 software for image capture.

DOXO sample was used as positive control. IC_{50} of La_2O_3-ZnO nanocomposite against MCF-7 was calculated based on a non-linear regression method. At least three individual experiments were

conducted. Results are shown as mean ± SD in Table 2, Figs. 5 and 6. By using one-way ANOVA, statistical significance was determined.

Table 2. Determination of MCF-7 cell viability over the treatment of test La_2O_3-ZnO nanocomposite

Conc. (µg/mL)	% Cell viability at 48 h	
	La_2O_3-ZnO	DOXO
1	97.11 ± 6.54	87.02 ± 7.04
5	90.58 ± 7.21	69.52 ± 5.74
10	81.89 ± 8.04	45.12 ± 3.11
20	65.12 ± 5.78	18.32 ± 1.63
30	47.12 ± 3.15	8.24 ± 1.01
40	31.11 ± 2.15	3.02 ± 0.47
50	17.04 ± 1.22	0.21 ± 0.05

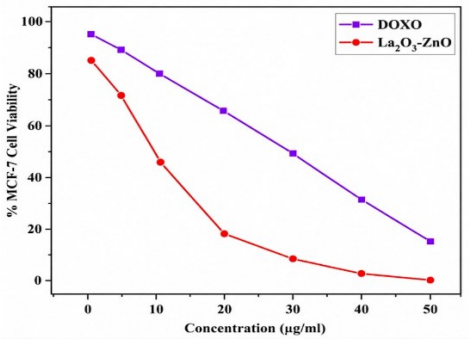


Figure 5. MCF-7 cell viability over the treatment test with La_2O_3-ZnO nanocomposite

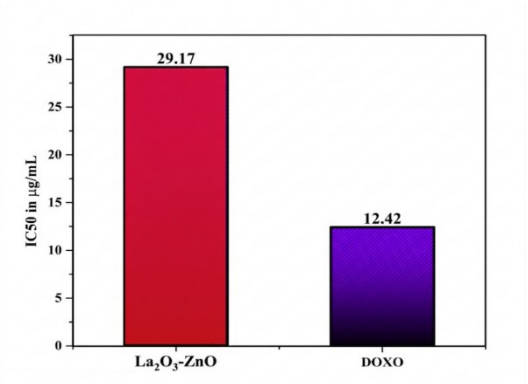


Figure 6. % Viability of MCF-7 over the treatment with La_2O_3-ZnO nanocomposite

RESULTS AND DISCUSSION

Consistent with the cytotoxicity results obtained from the MTT assay, both the synthesized La_2O_3-ZnO nanocomposite (lanthanum–zinc mixed oxide) and the reference drug DOXO caused noticeable morphological changes in MCF-7 cells, as shown in Figure 7. The analysis revealed that the La_2O_3-ZnO nanocomposite caused comparatively less morphological deformation in MCF-7 cells than that observed with DOXO treatment. Exposure to the lanthanum–zinc mixed oxide induced subtle morphological alterations, where the initially elongated spindle-shaped cells gradually became rounded and the intercellular spacing increased. In addition, increased cellular refraction was observed after treatment with the nanocomposite material.

.

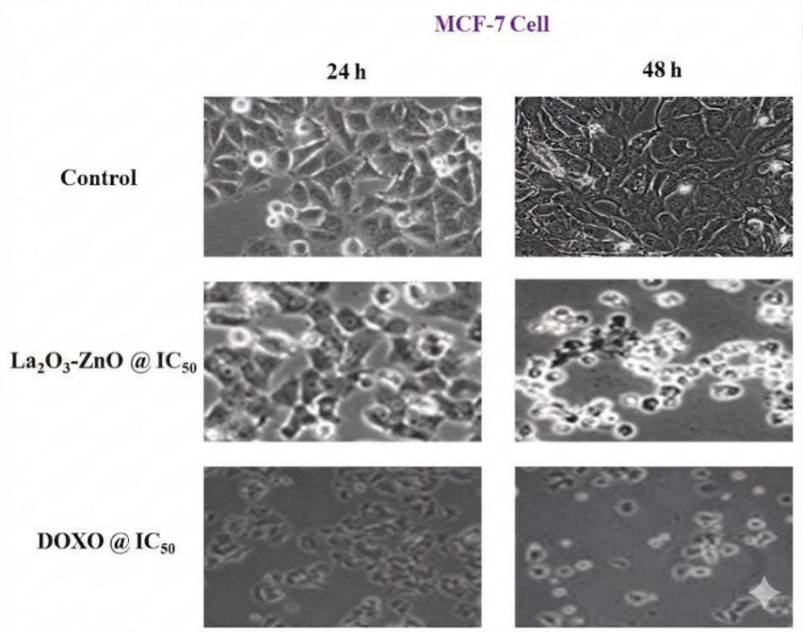


Figure 7. Morphological screening of MCF-7 cells over the treatment with La_2O_3-ZnO nanoparticles

The synthesized nanoparticles were further evaluated for their anticancer efficacy against the MCF-7 breast cancer cell line. Figure 7 illustrates the *in-vitro* activity profile and demonstrates the dose-dependent relationship between the synthesized lanthanum–zinc mixed oxide and anticancer activity. The study confirmed that the nanocomposite material produced comparatively moderate morphological distortion of MCF-7 cells relative to the severe cellular damage caused by DOXO. Specifically, treatment with the lanthanum–zinc mixed oxide resulted in gradual morphological modifications, including the transformation of spindle-shaped cells into rounded structures along with increased spacing between cells. The MTT assay results indicated that the synthesized nanoparticles exhibited moderate to good antiproliferative activity against MCF-7 breast cancer cells.

CONCLUSION

La_2O_3–ZnO mixed oxide nanoparticles were successfully synthesized using a simple co-precipitation technique. XRD analysis confirmed the crystalline nature of the nanocomposite with an average crystallite size of 30.79 nm, while UV-DRS analysis revealed band gap energy of 3.21 eV. FT-IR and SEM studies verified the formation of mixed metal oxide nanoparticles with porous nanocrystalline morphology. Cytotoxicity analysis demonstrated significant dose-dependent anticancer activity, the MCF-7 cell viability decreasing from 97.11 ± 6.54% at 1 µg/mL to 17.04 ± 1.22% at 50 µg/mL concentration. Morphological observations revealed cellular shrinkage, rounding, and structural deformation after nanoparticle treatment. The findings suggest that La_2O_3–ZnO nanocomposite possesses promising anticancer efficacy and may be considered as potential nanotherapeutic candidate for breast cancer treatment. Further investigations involving mechanistic studies, apoptosis pathway analysis, and *in-vivo* evaluations are recommended to establish its biomedical applicability and safety.

Acknowledgement: *The authors gratefully acknowledge Dr. Rafiq Zakaria, College for Women Aurangabad, Maharashtra, India for providing all required facilities for the research work. Authors also thank the Principal and Head of the Department of Chemistry, Jijamata College of Science and Arts, Bhende, Maharashtra, India for providing analysis facilities for the research work.*

Funding Support: *First author A. R. Padol heartily acknowledges for providing financial support from SARATHI, Maharashtra, India (Award No. 701/2022).*

Conflict of interest*: All authors hereby declare no conflict of interest.*

REFERENCES

1. D. Yuvaraj, R. Kaushik, K. Narasimha Rao, *ACS Applied Materials & Interfaces*, **2** (4), 1019 (2010), doi: 10.1021/am900792k.
2. Y. Wu, W. Jia, Q. An, Y. Liu, J. Chen, G. Li, *Nanotechnology*, **20** (24), 245101 (2009), doi: 10.1088/0957-4484/20/24/245101.
3. Y. Wang *et al.*, *Advanced Functional Materials*, **18** (7), 1131 (2008), doi: 10.1002/adfm.200701120.
4. W. K. Son, J. H. Youk, W. H. Park, *Carbohydrate Polymers*, **65** (4), 430 (2006), doi: 10.1016/j.carbpol.2006.01.037.
5. J.-P. Mosnier *et al.*, *Science and Technology of Advanced Materials*, **10** (4), 045003 (2009), doi: 10.1088/1468-6996/10/4/045003.
6. W. Jiang, H. Mashayekhi, B. Xing, *Environmental Pollution*, **157** (5), 1619 (2009), doi: 10.1016/j.envpol.2008.12.025.
7. Q. Li *et al.*, *Water Res,* **42** (18), 4591 (2008), doi: 10.1016/j.watres.2008.08.015.
8. M. Diao, M. Yao, *Water Res.,* **43** (20), 5243 (2009), doi: 10.1016/j.watres.2009.08.051.
9. A. Sharma et al., *Mater. Sci. Eng. C*, **165**, 115432 (2024).
10. S. Verma, P. Singh, *J. Alloys Compd.*, **987**, 178945 (2025).
11. M. Al-Harbi et al., *Ceram. Int.*, **51** (4), 11220 (2025).
12. R. K. Patel et al., *Nano-Struct. Nano-Objects*, **39**, 101245 (2024).
13. Y. Chen et al., *J. Nanobiotechology*, **24**, 55 (2026).
14. J. S. Kim *et al.*, *Nanomed.: Nanotechnol. Biol. Med.*, **3** (1), 95 (2007), doi: 10.1016/j.nano.2006.12.001.
15. Z. Huang *et al.*, *Langmuir*, **24** (8), 4140 (2008), doi: 10.1021/la7035949.
16. K. H. Tam *et al.*, *Thin Solid Films*, **516** (18), 6167 (2008), doi: 10.1016/j.tsf.2007.11.081.
17. E. Bae *et al.*, *Environ. Toxicol. Chem.*, **29** (10), 2154 (2009), doi: 10.1002/etc.278.
18. P. Huang *et al.*, *Environ. Toxicol. Pharmacol.* **31** (1), 25 (2011), doi: 10.1016/j.etap.2010.09.001.
19. G. A. H. Mekhemer, *Phys. Chem. Chem. Phys.*, **4** (21), 5400 (2002), doi: 10.1039/B204056P.
20. R. He *et al.*, *Nano Today*, **48**, 101694 (2023), doi: 10.1016/j.nantod.2022.101694.
21. B. Omran, K.-H. Baek, *Molecules*, **26** (22), 7031, (2021), doi: 10.3390/molecules26227031.
22. Q. Fan, X. Cui, H. Guo, Y. Xu, G. Zhang, and B. Peng, *J. Biomater. Appl.*, **35** (2), 237 (2020), doi: 10.1177/0885328220924540.
23. S. Keerthana, A. Kumar, *Crit. Rev. Toxicol.*, **50** (1), 47 (2020), doi: 10.1080/10408444.2020.1726282.
24. C. Picasso *et al.*, *Nanomater.*, **12** (13), 2265 (2022), doi: 10.3390/nano12132265.
25. Y. Mongy, T. Shalaby, et al., *Sci. Rep*., **14**, 13470 (2024). doi.org/10.1038/s41598-024-63258-7
26. S. A. Bhat, V. Kumar, D. S. Dhanjal, et al., *Discover Nano*, **19**, 121 (2024). https://doi.org/10.1186/

s11671-024-04072-y
27. J. B. Oehler, W. Rajapaksha, H. J.Albrecht, *Pers. Med,* **14**, (7), 723 (2024). https://doi.org/ 10.3390/jpm14070723
28. G. Ferro-Flores, A. Ancira-Cortez, B. Ocampo-García, L. Meléndez-Alafort, *Nanomater*., **14** (3), 296 (2024). https://doi.org/10.3390/nano14030296
29. S. Chandramohan, A. P. Francis, S. Pajaniradje, R. Rajagopalan, *Part. Sci. Technol*., **42** (7), 1155 (2024). https://doi.org/10.1080/ 02726351.2024.2364859
30. Z. Luo, Z. Yi, X. Liu, *Acc. Chem. Res.*, **56** (4), 425 (2023), doi: 10.1021/acs. accounts. 2c00681.
31. H. Wei *et al.*, *Adv. Opt. Mater.*, **11**, 11 (2023), doi: 10.1002/adom.202370037.
32. H. E. A. Mohamed *et al.*, *Appl. Organomet. Chem.,* **37** (6) (2023), doi: 10.1002/aoc.7091.
33. A. C. Albertsson, J., S. C. Abrahams, A. Kvick, *Acta Cryst.* B, **45**, 34 (1989), https://doi.org/10.1107/ S0108768188010109
34. Z. Lohberg, *Phys. Chem.,* **28**, 402 (1935).
35. H. Jamil *et al.*, *Thin Solid Films*, **732**, 138796 (2021), doi: 10.1016/j.tsf.2021.138796.
36. Z. N. Kayani, B. Amir, S. Riaz, S. Naseem, *Opt. Mater.*, **109**, 110287 (2020), doi: 10.1016/j.optmat. 2020.110287.
37. D. E. Navarro-López *et al.*, *Mater. Sci. Eng. C,* **123**, 112004 (2021), doi: 10.1016/j.msec.2021.112004.
38. P. Somu, H. D. Khanal, L. A. Gomez, R. Vinaykumar, J.-J. Shim, Y. R. Lee, *Biomass Conv. Bioref.* **15**, 22041 (2025), doi: 10.1007/s13399-022-03474-1.
39. R. L. Danhalilu, A. I. Kankara, S. M. Batagarawa, *Curr. J. Appl. Sci. Technol.,* **32** (2), 1 (2019), doi: 10.9734/CJAST/2019/46052.
40. M. I. Alahmdi *et al.*, *J. Inorg. Organomet. Polym. Mater.*, **32** (6), 2146 (2022), doi: 10.1007/s10904-022-02263-7.
41. A. A. Pathan, K. R. Desai, S. Vajapara, C. P. Bhasin, *Adv. Nanoparticles*, **07** (01), 28 (2018), doi: 10.4236/anp.2018.71003.
42. J. Mohanta, B. Dey, S. Dey, *ACS Omega*, **5** (27), 16510 (2020), doi: 10.1021/acsomega.0c00999.